Article

Optically programable quasi phase matching in four-wave mixing

Gil Bashan, Avishay Eyal, Moshe Tur & Ady Arie ✉

Quasi-phase matching (QPM) enhances nonlinear optical processes by compensating for phase mismatch, but traditional methods require permanent material modifications, limiting applicability in centrosymmetric media like standard optical fibers. We introduce the first efficient, optically controlled QPM in perturbative nonlinear optics, achieved through temporal modulation of counter-propagating pump waves. This induces a dynamic spatial modulation of nonlinear polarization in a polarization-maintaining fiber, enabling spatiotemporal QPM for four-wave mixing without altering the medium. We demonstrate broadband wavelength conversion across 298 nm—including the C- and L-bands of optical telecommunications—with a conversion efficiency of 5.4%. Our results also show tunable spectral shaping and wavelength agility through simple control of the pump waves. This reconfigurable, all-optical technique not only overcomes limitations of conventional QPM but also opens new possibilities for adaptable nonlinear optics. Potential applications span classical data processing, fiber sensing, quantum state control, and robust frequency conversion in dynamically programmable photonic systems.

Quasi-phase matching is a well-established technique utilized to enhance the efficiency of nonlinear optical processes[1–3]. It involves the spatial modulation of either linear or nonlinear polarization to achieve results akin to true phase matching[1–3]. While commonly employed in crystals and waveguides having second order nonlinearity through the spatial modulation of their nonlinear susceptibility[4–8], QPM can also be achieved by modulating linear polarization[9]. However, in centrosymmetric or amorphous materials, in which the dominant nonlinearity is of third order (characterized by the nonlinearity susceptibility tensor $\chi^{(3)}$), modulating the susceptibility is not feasible[3]. Nonetheless, several studies have demonstrated QPM in $\chi^{(3)}$ materials by deforming waveguides or optical fibers, thereby creating spatial modulation of the effective refractive index[10–14], birefringence[15], or by cascaded optical fibers[16,17].

In certain QPM generation methods, spatial modulation is achieved through optical processes, such as the photorefractive effect[9], photogalvanic effect[18–20], and optical controlling of ferroelectrics[7,8]. It is important to note that in all these techniques, the nonlinear pattern cannot be easily modified or erased once inscribed into the material, and at least several minutes are required to alter it.

A novel approach involving optically controlled QPM periods has been demonstrated in high harmonic generation in a hollow waveguide filled with ionized gas, exploiting the significant sensitivity of unbounded electrons involved in this unique process to changes in the accelerating field[21–24]. Several theoretical articles analyzed the extension of this method to the perturbative nonlinear optics regime, where pump lasers with moderate power levels are used[25,26]. In these studies, the proposed mechanism relies on sending the pump together with another light wave that counter-propagates with respect to the pump, forming a stationary interference pattern that modulates the nonlinear interaction. However, till now, constructive buildup of light along the nonlinear medium or a significant enhancement in efficiency was not demonstrated experimentally[27].

The standard QPM involves periodic changes of material properties, where the period determines the wavelength of the efficiency process[1–3]. Moreover, by altering the period or coupling strength of nonlinear polarization along the position, effects such as adiabatic frequency conversion[28–30], accumulation of adiabatic geometric phase[31,32], or controllable spectrum of efficiency of the nonlinear process[33,34], can be observed. Another possibility is to apply

School of Electrical Engineering, Faculty of Engineering, Tel Aviv University, Tel Aviv, Israel. ✉e-mail: ady@tauex.tau.ac.il

quasiperiodic modulation, thereby enabling to simultaneous phase match several processes[35–37].

Bragg-Scattering-Four wave mixing (BS-FWM) is a phase-sensitive parametric nonlinear process that enables efficient wavelength conversion over large wavelength shifts[3,38]. This process holds promise for a range of applications, including optical signal processing, optical spectrum analyzer, and wavelength translation[39,40]. In our study, we employ BS-FWM inside an optical fiber, in the regime of undepleted pumps. In this case, the dynamics of signal and idler waves is that of a two-level system, coupled by the two pump waves[32,41]. This enabled the demonstration of phenomena such as temporal Stern-Gerlach effect[42], Ramsey interference[43], and Hong-Ou-Mandel effect[44–46] in the frequency bin basis. FWM may also occur when the four waves differ in optical mode polarization and direction of propagation, leading to applications such as distributed fiber sensors of temperature, strain[47], and of media outside a standard fiber[48], as well as a new kind of isolator in fiber[49]. These effects are also being explored in integrated photonic platforms[50,51].

Here we propose and demonstrate the first optically controllable QPM in the perturbative nonlinear optics. Standard, unmodified polarization-maintaining (PM) fibers were utilized for the nonlinear optical medium. Two pumps, perpendicular in polarization, are both backward-propagating in the fiber, while signal and idler waves propagate in the forward direction. By controlling the pump's temporal modulation, spatial modulation along the fiber is achieved. This results in spatiotemporal modulation of the signal and idler nonlinear polarization, equivalent to QPM. Unlike standard QPM, where the nonlinear pattern is permanent in the optical medium, here, the optical medium remains unmodified while the optical fields involved in the nonlinear process are modulated instead. This feature allows us to demonstrate, on the same optical fiber, modification of the scattering wavelength across 300 nm (limited by our lab equipment), as well as shaping the phase matching spectrum with different functions such as Gaussian, the first Hermite-Gauss polynomial, and rectangular. Additionally, we demonstrate an efficiency of more than 5%.

Results
Theoretical model
In our theoretical framework, we consider two strong optical pump waves having orthogonal polarizations, with corresponding optical frequencies $\omega_p \pm \frac{\Omega}{2}$, co-propagating in a PM fiber along the negative z direction. Here, Ω represents the difference between the pumps polarized to the slow and fast axes. Weak signal and idler waves, polarized to the slow and fast axes, respectively, co-propagate along the positive z axis, i.e., in the opposite direction to the pumps. (Fig. 1).

Assuming undepleted pumps, where the fast (or slow) pump is time-modulated by a sinusoidal wave with angular frequency ω_m, we describe the evolution of the signal and idler wavepackets using coupled wave equations (CWE), akin to those seen in a two-level system[32]. The CWEs are: (for four-field model see Supplementary note 1):

$$\frac{\partial A_s}{\partial z} = i\gamma A_i A_p^f A_p^{s*} \cos(\kappa_m z + \omega_m t)\exp(i\Delta k z) \quad (1)$$

$$\frac{\partial A_i}{\partial z} = i\gamma A_s A_p^s A_p^{f*} \cos(\kappa_m z + \omega_m t)\exp(-i\Delta k z) \quad (2)$$

Here A_p^s, A_p^f, A_i, A_s represent the slowly varying complex envelopes of the pump waves polarized to the slow and fast axes, idler, and signal waves, respectively. Here t denotes time, and $\kappa_m = \frac{\omega_m}{c}n$ is the effective wavenumber of the modulation, where c is the speed of light, and n represents the average effective index along the two axes. The Kerr nonlinear coefficient is given by $\gamma = \frac{3\chi^{(3)}\omega}{8ncA_{eff}}$ and is expressed in units of $W^{-1}km^{-1}$, where $\chi^{(3)}$ is the third-order susceptibility of the fiber, ω is the optical angular frequency, and A_{eff} is the effective mode area. Since $n, \chi^{(3)}, \omega$, and A_{eff} are sufficiently close in value for all the optical fields considered, we approximate γ as being equal for all fields[52]. The wavenumber mismatch term is $\Delta k = k_p^f - k_p^s + k_i - k_s$, where k_p^f, k_p^s, k_s, k_i are the wavenumbers of the two pumps, signal, and idler, respectively (see in Fig. 2(a) illustration of the dispersion relation of the fiber).

In the standard case, where there is no pump modulation, i.e., $\omega_m = 0$ and $\kappa_m = 0$, energy conservation dictates the condition $\Omega = \omega_i - \omega_s$, where ω_i and ω_s denote the angular frequencies of the idler and signal waves. In this case, efficient conversion between the signal and idler waves occurs when their wavenumber mismatch is (approximately) $\Delta k(\Omega, \Delta\omega) \approx \frac{1}{c}(2\Omega n - \Delta n\Delta\omega)$ where Δn is the birefringence between the two principal axes, and $\Delta\omega$ is the offset between the signal optical frequency ω_s and the pump frequency ω_p^s (see supplementary note 1). We refer to this as the natural wavenumber
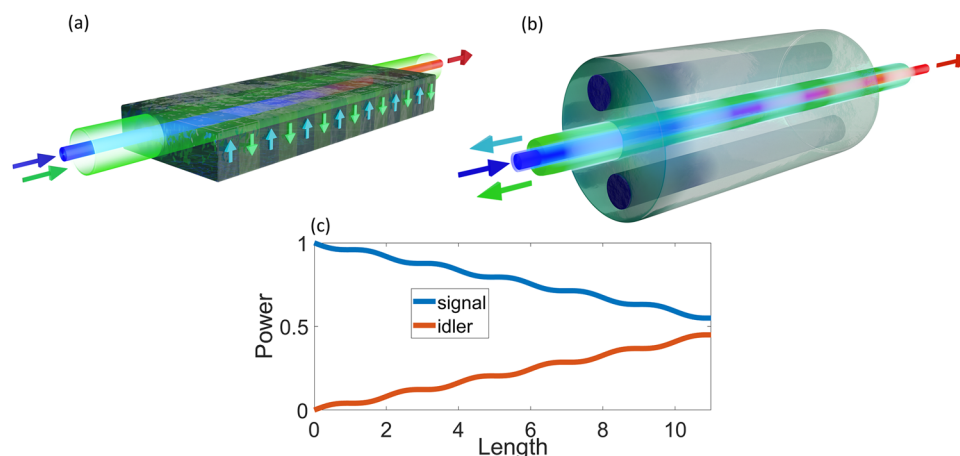

Fig. 1 | Conceptual comparison between standard and optically programmable QPM. In the case of standard QPM (**a**), spatial modulation of susceptibility within the optical medium is permanent. This modulation facilitates efficient conversion between input light (signal, indicated by a blue beam) and output light (idler, indicated by a red beam), which co-propagate from left to right and have different wavelengths. In the case of optically programmable QPM (**b**), the input light (signal wave) is coupled to an unmodified optical fiber that maintains uniformity along its length. Two pump waves involved in the nonlinear process counter-propagate relative to the signal and idler waves. Modulation of one of the pump waves (green beam) enables a process efficiency akin to standard QPM, facilitating the coherent buildup of the output light (signal wave) as illustrated in (**c**).
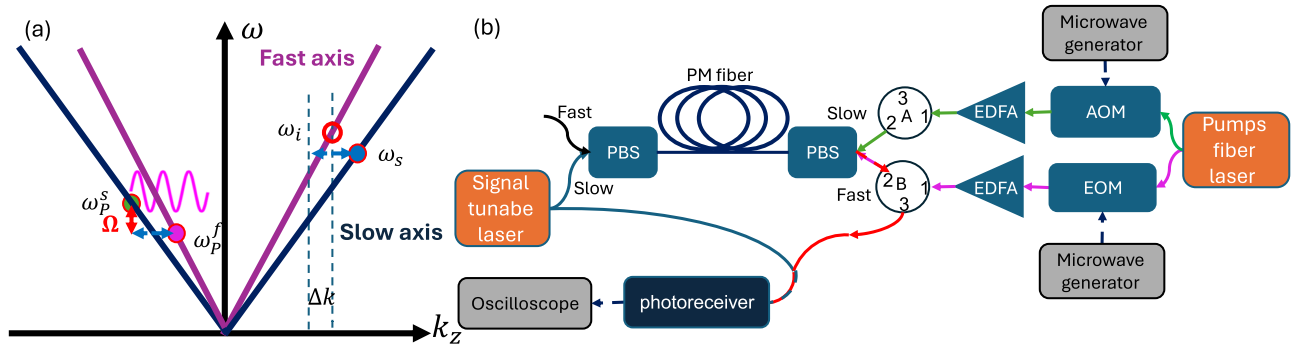
Fig. 2 | Phase-matching principle and experimental setup for optically programmable QPM. Panel (**a**) illustrates the dispersion relation between temporal frequency and axial wavenumber for light guided in the slow (dark blue) and fast (purple) axes of a polarization-maintaining (PM) fiber. The signal (represented by full blue circular markers) and the idler (represented by empty circular red marker) propagate forward along the slow and fast axes, respectively, while the slow and fast pump waves (represented by full green and violet circular markers, respectively) propagate backwards. The blue arrows represent the momentum difference between the two pumps, which results in a corresponding momentum mismatch Δk between the signal and the idler. The fast pump is modulated to create the optically programmable QPM that will align with the momentum mismatch. Panel (**b**) provides a schematic illustration of the experimental setup. AOM acousto-optic modulator, EOM electro-optic amplitude modulator, EDFA erbium-doped fiber amplifier, PBS polarization beam splitter.

mismatch. The corresponding angular frequency difference between the pump and signal is $\Delta\omega = 2\Omega\frac{n}{\Delta n}$.

When pump temporal modulation is applied with an angular frequency ω_m, Eqs. 1 and 2 resemble the standard QPM equations, where κ_m serves as the wavenumber of the spatial modulation. The temporal term in the sinusoidal wave induces QPM in energy, altering the frequency difference between the idler and signal waves, $\omega_i - \omega_s = \Omega \pm \omega_m$. This frequency shift introduces an additional term to the phase matching condition[53], $\Delta k_t = \frac{\omega_m}{c}n$, so the overall spatio-temporal term becomes:

$$\Delta k_{st} = \Delta k_t + \kappa_m = 2\frac{\omega_m}{c}n \tag{3}$$

(see supplementary note 1). The QPM is satisfied when $\Delta k_{st} = |\Delta k|$. Consequently, the pump-signal frequency difference with maximal coupling is:

$$\Delta\omega_{st}(\Omega, \omega_m) = (2\Omega \pm 2\omega_m)\frac{n}{\Delta n} \tag{4}$$

where the sign depends on the Fourier terms in $\sin(\kappa_m z + \omega_m t)$. This is a manifestation of spatiotemporal QPM[47], where the pump temporal modulation governs both the momentum mismatch Δk_{st} and the energy mismatch $\Delta\omega_{st}$. We note that the ratio $\frac{n}{\Delta n}$ is quite large (~4300 in our experiment), hence the frequency conversion can be achieved over very broad spectral range by relatively small change in the pump modulation frequency ω_m.

The interaction we consider includes two pump waves, but the wavelength of efficient coupling can be controlled by temporally modulating only one of the pumps with an angular frequency ω_m. Furthermore, by applying an additional envelope function $a(t)$ to the sinusoidal wave, nonuniform QPM can be created along the fiber. This enables to control the spectrum of the coupling efficiency, which can be represented as the Fourier transform $A(2\delta\frac{\Delta n}{n})$ of the envelope function $a(t)$, where δ is the frequency offset from the exact phase matching condition[33] (see Supplementary note 2).

The solution to the CWEs is the same as that of a two-level system[28,32]. Assuming initially zero idler power at the fiber's entrance, and completely satisfying the QPM condition, $\kappa_m = |\Delta k|$, the conversion efficiency to the idler at the fiber's end ($z = L$) is given by:

$$\eta = \frac{P_i(L)}{P_s(0)} = \sin^2\left(\sqrt{\frac{\gamma^2 P_p^s P_p^f}{4}}L\right) \tag{5}$$

Here, P_s, P_i, P_p^s, and P_p^f represent the signal, idler, slow pump, and fast pump powers, respectively. Note that the factor 1/4 in the sinusoidal argument accounts for the presence of two QPM orders (negative and positive), but only one is effective for each wavelength.

In the regime of relatively low efficiency, where $\sqrt{\frac{\gamma^2 P_p^s P_p^f}{4}}L \ll 1$, the sine function can be approximated as a linear function. Under this approximation, the conversion efficiency simplifies to $\eta \approx \frac{\gamma^2 P_p^s P_p^f}{4}L^2$.

Experimental results

The optically programable QPM setup is illustrated in Fig. 2. The pump waves were generated from a fiber laser at 1550 nm, which was split into two branches, and both of them coupled to the exit port of the fiber, $z = L$. In one branch, the optical wave was upshifted by a fixed intermediate frequency offset of $\frac{\Omega}{2\pi} = 200$ MHz using an acousto-optic modulator. This served as the non-modulated pump and was coupled to the slow axis of 30 m panda-type PM fiber via a circulator A, and polarization beam splitter (PBS). In the other branch, modulation was applied to the second pump by an electro-optic modulator driven by an arbitrary waveform generator and coupled to the fast axis of the fiber from the same edge via circulator B. The modulator is biased to the minimum power operating point, where the optical field response is linear with respect to the applied voltage. The average power of each of the two pumps was amplified to 80 mW.

A continuous-wave signal wave from a tunable diode laser was also split into two branches. One branch served as a local oscillator (LO), while the other, serving as the signal wave, was coupled to the slow axis of the PM fiber from the entrance port of the fiber, $z = 0$. Owing to the nonlinear interaction, part of the signal wave was converted to the orthogonally polarized idler, which propagated through the fast arm of the PM fiber and was sent using the PBS and circulator B towards a PM coupler, where it was mixed with the LO and detected using a photoreceiver, over acquisition time of $\Delta\tau$. Prior to detection, both the LO and idler passed through optical bandpass filters to suppress any residual pump leakage (the bandpass filters are not shown in the setup). The Fourier Transform $\tilde{V}(\omega)$ of the detected voltage $v(t)$
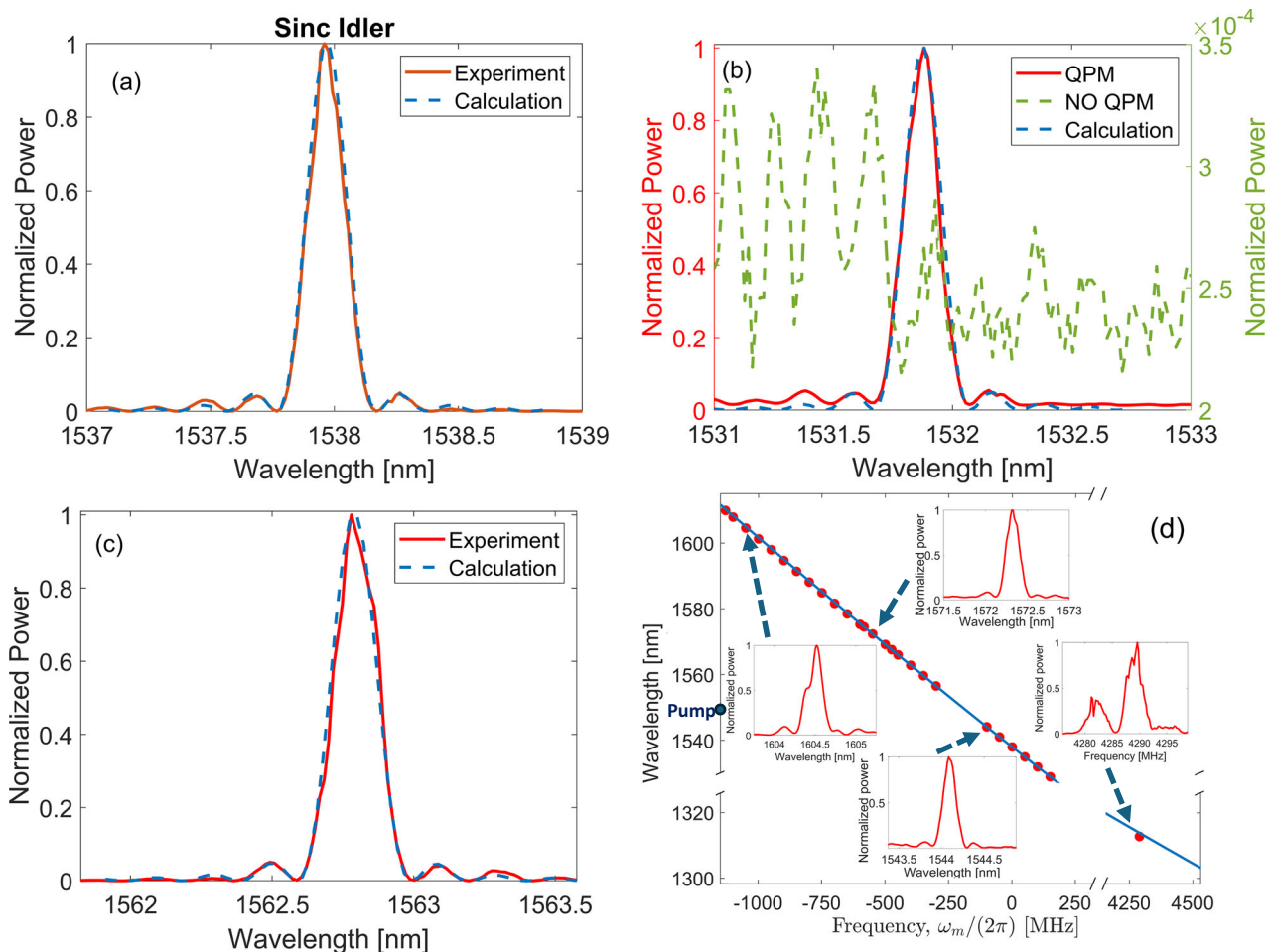
Fig. 3 | Experimental and theoretical demonstration of wavelength-tunable signal-idler coupling via optically programmable QPM. a presents the normalized signal-idler coupling spectrum under natural phase matching conditions, where no QPM is applied. The red line represents experimental data, while the well-matched, dashed blue line depicts numerical calculations. Panel (b) illustrates the same scenario as **a** but with a QPM frequency of $\omega_m/2\pi$ = 100 MHz. The green line represents the signal-idler coupling without QPM. A striking difference of more than three orders of magnitude is observed between coupling with and without QPM. **c** mirrors **a** and **b** but with a QPM frequency of $\omega_m/2\pi$ = 400 MHz. Here, the maximum coupling occurs near 1562.8 nm, corresponding to the negative order of the QPM. **d** summarizes 27 measurements conducted with different QPM frequencies $\omega_m/2\pi$ ranging from 50 MHz to 4.3 GHz. The graph demonstrates the tunability of the spectrum over a wide range of 298 nm. The insets show examples of the measurements that contribute to the main graph. The red markers represent the experimental measurements, while the blue line corresponds to the theoretical analysis. According to the theory, the optical frequency is linearly dependent on the QPM frequency (see Eq. 4). The theoretical line has linear dependence on frequency (Eq. 4), but since it is shown here as a function of wavelength, its slope varies.

was analyzed offline, and the square of Fourier Transform magnitude $\left|\widetilde{V}(\Omega \pm \omega_m)\right|^2$ was proportional to the idler power.

Figure 3 depicts the idler normalized output power as a function of wavelength for various QPM frequencies. In all panels of Fig. 3, the acquisition time was $\Delta\tau = 1\mu s$, and the absolute value of the Fourier Transform of the voltage $|V(\omega)|$ was averaged offline over 256 times. We fine-tuned the pump wavelength in the simulation by tens of picometers to precisely match the experimental conditions and eliminate any wavelength drifting effects. Panel (a) presents the idler power without any QPM, with the maximum coupling near 1538 nm corresponding to a birefringence of $\Delta n \approx 3.4 \times 10^{-4}$. The dashed line represents numerical calculations (see details in the method section). Panel (b) shows the same for a QPM frequency of $\omega_m/2\pi$ = 100 MHz, with the maximum coupling near 1532 nm. Panel (c) is analogous to panel (a) but with a QPM of $\omega_m/2\pi$ = 400 MHz, resulting in maximum coupling near 1562 nm. Here, the wavelength of maximum coupling is above the natural phase-matching wavelength observed in panel (a), as the phase matching is due to the negative order of the QPM. Panel (d) presents the wavelength of maximum coupling as a function of the

QPM frequency, with negative frequencies indicating the negative (−1) order of QPM. The red markers present measurements, while the blue line presents theoretical analysis. As shown in the figure, by varying the QPM frequency by less than 800 MHz, phase matching can be achieved over a spectral range of 80 nm, covering the entire C-band and L-band of optical telecom. Additionally, we demonstrate coupling at 1312 nm. In this experiment, as shown in the rightmost inset, we did not vary the signal wavelength (as in the other experiments) but instead swept over the QPM frequency and found maximum coupling near 4.3 GHz. Together, these experiments demonstrate tunability over a spectral range of 298 nm. The deviation from the ideal sinc function is attributed to inhomogeneities in the fiber's birefringence along its length[48].

Figure 4 demonstrates the impact of adding an envelope modulation to the sinusoidal wave, which in turn modulates the pump, with various pulse shapes. The normalized coupling spectrum is depicted when the QPM frequency is $\omega_m/2\pi = 100$ MHz. In all panels, the absolute value of the Fourier Transform of the voltage $|V(\omega)|$ was averaged offline over 512 repeating pump pulses. The experimental data in all panels is represented by a solid red line, while the dashed
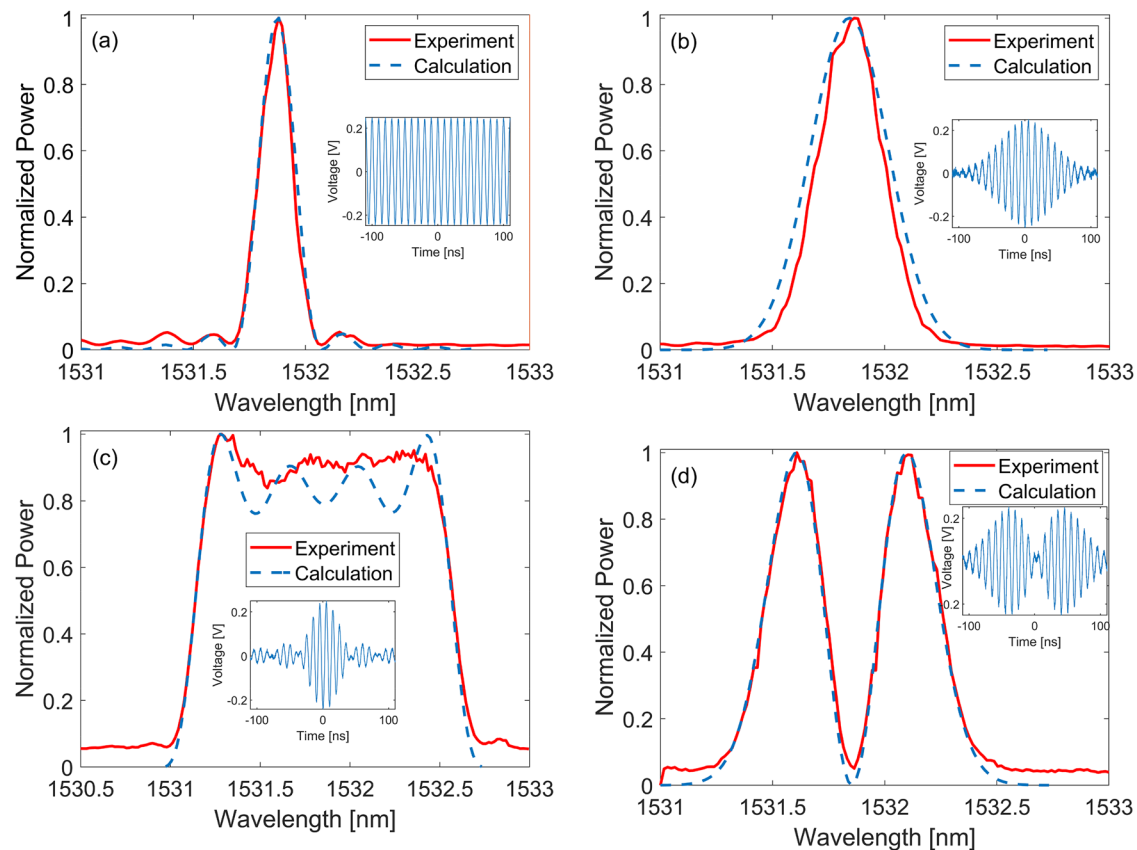
Fig. 4 | Signal-Idler coupling spectra with various pulse shapes. a Normalized spectrum of idler power when the fast pump is modulated by a pure sinusoidal wave of $\frac{\omega_m}{2\pi} = 100$ MHz. The spectrum exhibits a sinc shape, corresponding to the Fourier transform of a rectangular function (over a 30 m PM fiber). Experimental data is represented by the solid red line, while numerical calculations are depicted by the dashed blue line. **b–d** replicate the scenario presented in (**a**), with the sinusoidal wave modulated by Gaussian, sinc, and the first Hermite-Gauss polynomial, respectively. In each case, the measured spectra represent the Fourier transform of the respective pulse shape: Gaussian for **b**, rectangular for **c**, and the first Hermite-Gauss polynomial for **d**. Inset graphs in each panel display the temporal voltage waveform used to modulate the fast pump light, illustrating the pulse shapes applied.

line represents the simulation. We adjusted the pump wavelength in the simulation by tens of picometers to match the experiment and prevent wavelength drifting effects. The pulse duration was 40 ns in all panels, denoted by T. The insets in all panels correspond to the generated arbitrary waveform voltage before amplification. In **a**, where there is no envelope modulation to the sine wave, the spectrum is simply governed by the length of the PM fiber and takes the shape of the sinc function. The acquisition time for this panel was $\Delta\tau = 1\mu s$. For b–d, the acquisition time was $\Delta\tau = 20ns$, synchronized with the arbitrary waveform generator. In panel (b), the sinusoidal wave was modulated by a Gaussian pulse $a(t) = \exp\left(-\frac{1}{2}\left(\frac{t}{T}\right)^2\right)$. As expected, the spectrum resembles the Fourier Transform of the pulse, which is also Gaussian. Panel (c) features a pulse shape characterized by the normalized sinc function $a(t) = \sin\left(\frac{\pi t}{T}\right)/\frac{\pi t}{T}$, resulting in a rectangular coupling spectrum. In panel (d), the pulse shape corresponds to the first Hermite-Gauss polynomial, $a(t) = t \times \exp\left(-\frac{1}{2}\left(\frac{t}{T}\right)^2\right)$, with the resulting spectrum also displaying the dual-lobe Hermite-Gauss characteristics.

Figure 5 illustrates the conversion efficiency to the idler wave as a function of the pump power. In panel (a), the PM fiber mirrors the parameters outlined in Figs. 4 and 3, spanning a length of 30 meters, with the signal power set at 3 mW and the fast pump power maintained at 670 mW. The slow pump power is monotonically varied from 30 to 300 mW. Experimental data, denoted by the solid red line, closely aligns with theoretical calculations represented by the dashed blue line. Notably, the data indicate a maximum efficiency of 7.5×10^{-3} %. In panel (b), a shift

is observed as the PM fiber transitions to a 440 m PM panda-type fiber. Here, the fast pump power is held constant at 1 W, while the fast pump power undergoes adjustments from 180 mW to 1 W. The maximum efficiency attained in this configuration reaches 5.4%. The pump light source is broadened to 300 MHz through phase modulation via pseudo-random binary sequence, in order to mitigate the influence of spontaneous Brillouin scattering, that may limit the process efficiency. Theoretical underpinnings, corroborated by experimental findings, delineate a clear relationship between efficiency, fiber length, and pump power. Specifically, in relatively low efficiency $\eta \ll 1$, the efficiency is shown to scale quadratically with the fiber length and linearly with each of the pump powers, aligning with established theoretical frameworks and empirical observations. The partial discrepancy between the measurement and the theoretical model in panel (b) is due to a lack of uniformity in the birefringence along the fiber[48] which leads to an effective interaction length that is shorter than the actual physical length of the fiber. Data analysis indicates that the effective length in this case is 356 m.

The measured efficiency, even at the high pump power, justifies our assumption of the undepleted pump approximation. However, with higher conversion efficiency, this analysis can be further extended to the depleted pump regime[32].

Discussion

Wavelength tunability of the signal-to-idler coupling has been achieved over a spectral range of 298 nm, including a dense sampling of the entire telecom C-band and L-band, and limited only by the lab equipment. Control over the wavelength is achieved by modulating
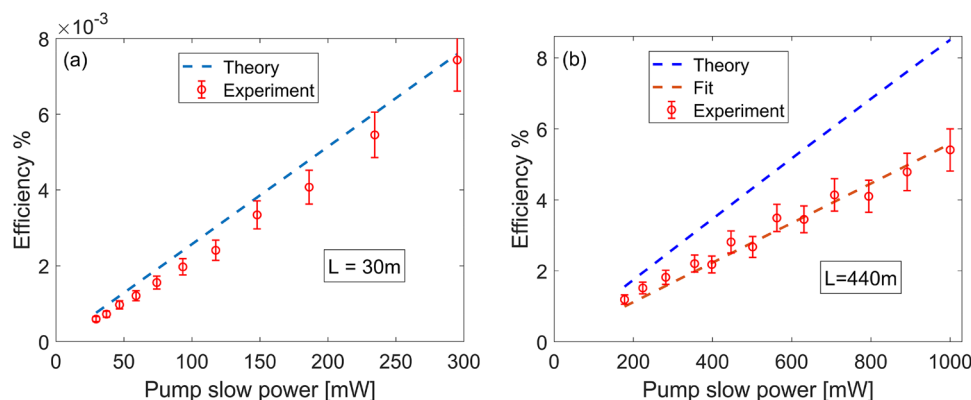
Fig. 5 | Efficiency dependence on slow pump power for short and long fibers. **a** illustrates the efficiency of the process as a function of slow pump power, with the fast pump set at 670 mW and the fiber length at 30 m. Experimental data is depicted by the red markers, which include vertical error bars representing the standard deviation, while theoretical analysis is represented by the dashed blue line. **b** mirrors **a** but with the fast pump fixed at 1 W. Additionally, the fiber length is extended to 440 m. The dashed red line is a fit to the experimental data, indicating an effective length of 356 m.

the frequency of the pump, typically in the range of hundreds of MHz. Moreover, alongside wavelength tunability, spectrum shaping has been demonstrated by modulating the envelope of one of the pump waves. The shape of the spectrum corresponds to the Fourier Transform of the pump pulse, showcasing shapes such as Sinc, Gaussian, first-order Hermite-Gauss polynomial, and rectangular.

The demonstrated efficiency of the nonlinear coupling was 5.4% for a 440 m fiber. However, this efficiency scales approximately with the square of the length and linearly with each pump power. Longer PM fibers of a few km are commercially available and commonly used in fiber optics gyroscopes, which can potentially bring the efficiency close to unity. Nevertheless, in long lengths and with high pump powers, the presence of spontaneous Brillouin scattering may limit efficiency. To address this challenge, it is possible to broaden the pump wave's source linewidth[54], albeit limited by walk-off between the two optical modes. Additionally, another approach to mitigate Brillouin scattering is to employ anti-guiding acoustic wave optical fibers[55].

When a spectral envelope is applied to modulate the QPM pattern, the effective interaction length is reduced, leading to lower nonlinear conversion efficiency. However, this spectral shaping relaxes constraints on the pump power, such as EDFA gain saturation and Brillouin scattering thresholds, thus allowing higher pump powers that can partly compensate for the efficiency reduction. Furthermore, although in principle the efficiency depends only weakly on wavelength, in practice, deviations from the 1550 nm working point increase the sensitivity to fiber inhomogeneities, which may degrade efficiency.

The response time of the optically programmable QPM is determined by the signal's time of flight in the fiber, which is on the order of only microseconds. This is many orders of magnitude faster than any other optically-based method to modify the nonlinearity[9,19]. The method offers efficient conversion over an extremely broad range of wavelength difference between the pump and signal, shown here up to 300 nm. We note that the signal-idler frequency difference was still limited to only 4.5 GHz, but this is by no means a fundamental limitation. In our experiment, the frequency difference between the two pumps ($\Omega = 200 MHz$) is multiplied by ~4300; hence larger difference would generate an idler frequency in wavelength ranges that we cannot measure. However, it is possible to significantly increase Ω, and subsequently the difference between the signal and the idler while remaining in the infrared regime by either using fiber with higher birefringence[56], or alternatively by using two different modes of a few-mode fiber having different propagation constants[57] thereby achieving a signal-idler wavelength difference on the order of tens nanometers. For example, in a photonic crystal fiber with a birefringence of $\Delta n = 8.795 \times 10^{-2}$[56], a frequency difference of $\frac{\Omega}{2\pi} = 3.1 THz$ (26 nm)

between the pumps near 1560 nm, with a modulation frequency of $\omega_m/2\pi = 10 GHz$, is suitable for phase matching signal and idler waves with a frequency separation of $\frac{\Omega + \omega_m}{2\pi} = 3.11 THz$ near 1000 nm.

The optically programmable QPM holds promise for applications such as frequency and polarization conversion. Furthermore, its straightforward integration into distributed fiber sensors can enable monitoring of temperature, strain, or chemical liquids outside the fiber[47,48]. Moreover, the ability to control the coupling spectrum demonstrated here may also be utilized for all-optical pulse shaping. In particular, ultra-broadband spectra can be achieved by tailoring the pump envelope into a short pulse; however, the pulse duration cannot be made arbitrarily short, as it will ultimately be limited by chromatic dispersion.

The optically programmable QPM scheme relies on the third-order Kerr nonlinearity, which is inherent to all optical materials and does not require to use non-centro symmetric materials[3]. This universality enables the implementation of the technique in a wide range of waveguides, including silicon and silicon nitride platforms[58], as long as the waveguide supports at least two true optical modes, which may share the same polarization or differ in polarization. Furthermore, the concept can be extended to other nonlinear mechanisms, such as Coherent Anti-Stokes Raman Scattering[59].

By using a wideband spectral signal, such as an amplified spontaneous emission source, the precise QPM frequency can directly control the idler output wavelength. Since the RF modulation can be finely controlled, the result is a fast and precisely tunable source (as we have demonstrated for example in measuring the conversion efficiency near 1312 nm, see inset in Fig. 3d), which can be valuable for various applications, such as optical frequency-domain reflectometry, where linear optical-frequency modulation is required[60], as well as spectroscopy of atomic and molecular transitions and characterization of resonant optical structures. Additionally, we have so far demonstrated stimulated FWM by sending two pumps and a signal into the fiber; however, it is also possible to use the optically programmable QPM for spontaneous FWM, where only two fields, the signal and the slow pump, are injected, while the other pump and the idler are generated within the fiber. This can be useful as a frequency-bin quantum source for applications in quantum information[61]

While in this work the central modulation frequency of the pump wave was fixed throughout the interaction, it is possible to facilitate methods from optical coherent control, such as adiabatic frequency conversion[28-30] and adiabatic geometrical phase accumulation[31,32] by varying the modulation frequency along the interaction. Adiabatic processes offer advantages in the realm of broadband and robust frequency conversion and enable precise control of the optical state[28-30]. In the context of FWM, the adiabatic condition requires

that $\left|\frac{d\Delta k}{dz}\right| \ll \frac{\left(\Delta k^2 + \gamma^2 P_p^s P_p^f\right)^{\frac{3}{2}}}{\gamma \sqrt{P_p^s P_p^f}}$, Satisfying this condition requires both sufficiently strong coupling and a long enough interaction length[28]. This can be achieved by using highly nonlinear fibers and leveraging anti-guiding acoustic wave optical fibers, as discussed earlier. Additionally, in adiabatic frequency conversion, the process begins in one eigenstate of the system and ends in the other. Therefore, the phase mismatch Δk should start with a large magnitude and one sign, and gradually evolve to a large magnitude with the opposite sign by the end of the interaction.

In summary, optically programmable QPM has been experimentally demonstrated. Our work represents the first experimental demonstration of spatiotemporal quasi phase matching in the perturbative nonlinear optical regime, where the pump modulation controls both the momentum conservation and energy conservation conditions. Measurements were conducted using standard optical telecom components and commercial, unmodified panda-type PM fiber. Unlike other types of QPM in the perturbative regime, no modification of the optical medium is required. The key to this form of QPM lies in modulating the light waves involved in the nonlinear process and utilizing counter-propagation to convert temporal modulation into spatial modulation.

Methods

Numerical simulation

This study employs a rigorous simulation framework, utilizing the Euler method[62], to analyze the dynamics of two pump waves, the signal wave, and the idler wave within a fiber-optic system. The propagation scenario involves two pump waves propagating to one side, while the signal and idler waves propagate to the other side of the fiber.

Since the simulation calculates fields propagating in opposite directions, the initial condition must encompass the entire fiber. Initially, the signal wave is configured as a continuous wave spanning the entire length of the fiber, while the idler and the two pump waves are set to zero intensity throughout. The modulation of the pump waves is meticulously adjusted to match the specific experimental conditions under investigation.

Key parameter values utilized in the simulation include an average effective index $n = 1.448$, a birefringence between the two principal axes $\Delta n = 3.75 \times 10^{-4}$, a Kerr nonlinear coefficient $\gamma = 1.3 W^{-1} km^{-1}$, and a loss coefficient $\alpha = 0.2 dB/km$.

A detailed spatiotemporal visualization of the four optical fields (fast pump, slow pump, signal, and idler) is provided in Supplementary Fig S1, illustrating their evolution over a 31.5 m fiber and a 334 ns simulation window, with a fast pump modulation frequency of 25 MHz. The time required to reach steady state is approximately twice the light propagation time through the fiber. This duration accounts for the time needed for the fast pump to fill the entire fiber, followed by the time it takes for the signal wavefront to traverse the fiber.

Experimental setup

The experimental setup consisted of a counter-propagating configuration in a polarization-maintaining (PM) fiber. Two pump waves were injected into one end of the fiber, while a tunable signal wave was launched into the opposite end. The fast pump was generated by a fiber laser with a linewidth $< 1 kHz$ (NKT-Koheras ADJUSTIK), and the slow pump was derived from the same source using an optical coupler and frequency-shifted using an acousto-optic modulator (AA Optoelectronics MT200-IIR30-Fio). The signal was produced using a tunable external cavity laser with a linewidth of 100 kHz (Yenista OSCIS AG C-band W). For experiments probing the response near 1312 nm, a laser with a linewidth of 10 MHz (ORTEL 3541 C) was used.

Temporal modulation of the fast pump was performed using an electro-optic amplitude modulator with a 10 GHz cut-off frequency

(Photline MXER-LN-10), driven by an arbitrary waveform generator. All optical beams were polarization-aligned to their respective fiber axes using polarization controllers and fiber-based polarization beam splitters before being coupled into the PM fiber (Corning PM fiber 15-U40A). The fiber length ranged from 30 m to 440 m depending on the specific experiment, and its birefringence was $\Delta n \approx 3.75 \times 10^{-4}$, as determined from experimental measurement.

For detection, the signal and idler outputs were directed to either a fast photoreceiver or an optical spectrum analyzer. The photoreceiver had a responsivity of 40,000 V/W and a rise time of 0.2 ns. Its electrical output was digitized using a high-speed oscilloscope operating at 1 GSa/s. In experiments measuring conversion efficiency, both the signal and idler were recorded using an optical spectrum analyzer with a resolution of 0.8 pm, allowing accurate spectral resolution and effective suppression of background leakage into the fast axis.

Data availability
All data appears in the main text or supplementary materials.

References

1. Armstrong, J. A., Bloembergen, N., Ducuing, J. & Pershan, P. S. Interactions between Light Waves in a Nonlinear Dielectric. *Phys. Rev.* **127**, 1918–1939 (1962).
2. Fejer, M. M., Magel, G. A., Jundt, D. H. & Byer, R. L. Quasi-phase-matched second harmonic generation: tuning and tolerances. *IEEE J. Quantum Electron.* **28**, 2631–2654 (1992).
3. Boyd, R. W. *Nonlinear Optics* (Academic Press, 2003).
4. Wang, C. et al. Ultrahigh-efficiency wavelength conversion in nanophotonic periodically poled lithium niobate waveguides. *Optica* **5**, 1438–1441 (2018).
5. Timurdogan, E., Poulton, C. V., Byrd, M. & Watts, M. Electric field-induced second-order nonlinear optical effects in silicon waveguides. *Nat. Photon.* **11**, 200–206 (2017).
6. Lu, J., Li, M., Zou, C.-L., Al Sayem, A. & Tang, H. X. Toward 1% single-photon anharmonicity with periodically poled lithium niobate microring resonators. *Optica* **7**, 1654–1659 (2020).
7. Wei, D. Z. et al. Experimental demonstration of a three-dimensional lithium niobate nonlinear photonic crystal. *Nat. Photon.* **12**, 596–601 (2018).
8. Xu, T. X. et al. Three-dimensional nonlinear photonic crystal in ferroelectric barium calcium titanate. *Nat. Photon.* **12**, 591–595 (2018).
9. Horowitz, M., Bekker, A. & Fischer, B. Broadband second-harmonic generation in $Sr_xBa_{1-x}Nb_2O_6$ by spread spectrum phase matching with controllable domain gratings. *Appl. Phys. Lett.* **62**, 2619–2621 (1993).
10. Lavdas, S. et al. Wavelength conversion and parametric amplification of optical pulses via quasi-phase-matched four-wave mixing in long-period Bragg silicon waveguides. *Opt. Lett.* **39**, 4017–4020 (2014).
11. Tarnowski, K., Kibler, B., Finot, C. & Urbanczyk, W. Quasi-phase-matched third harmonic generation in optical fibers using Refractive-Index Gratings. *IEEE J. Quantum Electron.* **47**, 622 (2011).
12. Driscoll, J. B. et al. Width-modulation of Si photonic wires for quasi-phase-matching of four-wave-mixing: experimental and theoretical demonstration. *Opt. Express* **20**, 9227–9242 (2012).
13. Lühder, T. A. et al. Tailored multi-color dispersive wave formation in quasi-phase-matched exposed core fibers. *Adv. Sci.* **9**, 2103864 (2022).
14. Hickstein, D. D. et al. Quasi-phase-matched supercontinuum generation in photonic waveguides. *Phys. Rev. Lett.* **120**, 053903 (2018).
15. Murdoch, S. G., Leonhardt, R., Harvey, J. D. & Kennedy, T. A. B. Quasi-phase matching in an optical fiber with periodic birefringence. *JOSA B* **14**, 1816–1822 (1997).

16. Kim, J., Boyraz, O., Lim, J. H. & Islam, M. N. Gain enhancement in cascaded fiber parametric amplifier with quasi-phase matching: theory and experiment. *J. Light. Technol.* **19**, 247–251 (2001).

17. Sternklar, S. et al. Quasi-phase-matched generation of optical intensity waves. *Opt. Lett.* **31**, 2894–2896 (2006).

18. Nitiss, E., Hu, J., Stroganov, A. & Brès, C. S. Optically reconfigurable quasi-phase-matching in silicon nitride microresonators. *Nat. Photon.* **16**, 134–141 (2022).

19. Billat, A. et al. Large second harmonic generation enhancement in Si_3N_4 waveguides by all-optically induced quasi-phase-matching. *Nat. Commun.* **8**, 1016 (2017).

20. Hickstein, D. D. et al. Self-organized nonlinear gratings for ultrafast nanophotonics. *Nat. Photon.* **13**, 494–499 (2019).

21. A. Zhang, X. et al. Quasi-phase-matching and quantum-path control of high harmonic generation using counterpropagating light. *Nat. Phys.* **3**, 270–275 (2007).

22. Cohen, O. et al. Grating-assisted phase matching in extreme nonlinear optics. *Phys. Rev. Lett.* **99**, 053902 (2007).

23. Shoulga, G. & Bahabad, A. Simultaneous ultrabroadband quasi-phase-matching for high-order harmonic generation. *Phys. Rev. A* **99**, 043813 (2019).

24. Shoulga, G., Barir, G. R., Katz, O., & Bahabad, A. All-optical spatio-temporal phase-matching of high harmonic generation using a traveling-grating pump field. *Appl. Phys. Lett.* **122** (2023).

25. Bahabad, A., Cohen, O., Murnane, M. M. & Kapteyn, H. C. Quasi-phase-matching and dispersion characterization of harmonic generation in the perturbative regime using counterpropagating beams. *Opt. express* **16**, 15923 (2008).

26. Lytle, A. L., Dyke, E., Novella, J., Branch, T. & Gagnon, E. Broadband second harmonic generation of counter-propagating ultrashort pulses. *Opt. Express* **30**, 17922–17935 (2022).

27. Lytle, A. L., Camuccio, R., Myer, R., Penfield, A. & Gagnon, E. Influence of counterpropagating light on phase matching in second-harmonic generation. *JOSA B* **33**, 1538–1542 (2016).

28. Suchowski, H., Oron, D., Arie, A. & Silberberg, Y. Geometrical representation of sum frequency generation and adiabatic frequency conversion. *Phys. Rev. A* **78**, 063821 (2008).

29. Suchowski, H., Porat, G. & Arie, A. Adiabatic processes in frequency conversion. *Laser Photonics Rev.* **8**, 333–367 (2014).

30. Moses, J., Suchowski, H. & Kärtner, F. X. Fully efficient adiabatic frequency conversion of broadband Ti:sapphire oscillator pulses. *Opt. Lett.* **37**, 1589–1591 (2012).

31. Karnieli, A. & Arie, A. Fully controllable adiabatic geometric phase in nonlinear optics. *Opt. Express* **26**, 4920 (2018).

32. Li, Y., Lü, J., Fu, S. & Arie, A. Geometric representation and the adiabatic geometric phase in four-wave mixing processes. *Opt. Express* **29**, 7288–7306 (2021).

33. Shiloh, R. & Arie, A. Spectral and temporal holograms with nonlinear optics. *Opt. Lett.* **37**, 3591–3593 (2012).

34. Galvanauskas, A., Harter, D., Arbore, M. A., Chou, M. H. & Fejer, M. M. Chirped-pulse-amplification circuits for fiber amplifiers, based on chirped-period quasi-phase-matching gratings. *Opt. Lett.* **23**, 1695–1697 (1998).

35. Zhu, S. N., Zhu, Y. Y. & Ming, N. B. Quasi-phase-matched third-harmonic generation in a quasi-periodic optical superlattice. *Science* **278**, 843–846 (1997).

36. Lifshitz, R., Arie, A. & Bahabad, A. Photonic quasicrystals for nonlinear optical frequency conversion. *Phys. Rev. Lett.* **95**, 133901 (2005).

37. Fradkin-Kashi, K. & Arie, A. Multiple-wavelength quasi-phase-matched nonlinear interactions. *IEEE J. Quantum Electron* **35**, 1649–1656 (1999).

38. Provo, R., Murdoch, S., Harvey, J. D., & Méchin, D., *Opt. Lett.* **35**, 3730–3732 (2010).

39. Méchin, D., Provo, R., Harvey, J. D. & McKinstrie, C. J. 180-nm wavelength conversion based on Bragg scattering in an optical fiber. *Opt. Express* **14**, 8995–8999 (2006).

40. Li, B., Wei, Y., Kang, J., Zhang, C., & Wong, K. K. Parametric spectrotemporal analyzer based on four-wave mixing Bragg scattering. *Opt. Lett.* **43**, 1922–1925 (2018).

41. Ding, X. et al. Observation of rapid adiabatic passage in optical four-wave mixing. *Phys. Rev. Lett.* **124**, 153902 (2020).

42. Bashan, G., Eyal, A., Tur, M. & Arie, A. All-optical Stern-Gerlach effect in the time domain. *Opt. Express* **32**, 9589–9601 (2024).

43. Clemmen, S., Farsi, A., Ramelow, S. & Gaeta, A. L. Ramsey interference with single photons. *Phys. Rev. Lett.* **117**, 223601 (2016).

44. Joshi, C. et al. Frequency-domain quantum interference with correlated photons from an integrated microresonator. *Phys. Rev. Lett.* **124**, 143601 (2020).

45. Imany, P. et al. Frequency-domain Hong–Ou–Mandel interference with linear optics. *Opt. Lett.* **43**, 2760 (2018).

46. Kobayashi, T. et al. Frequency-domain Hong–Ou–Mandel interference. *Nat. Photon.* **10**, 441–444 (2016).

47. Liu, L. et al. Distributed temperature–strain sensor based on inter-mode Kerr four-wave mixing of PMF: proposal and proof-of-concept. *Appl. Phys. Express* **15**, 072003 (2022).

48. Sharma, K. et al. Direct time-of-flight distributed analysis of nonlinear forward scattering. *Optica* **9**, 419–428 (2022).

49. Bashan, G. et al. Forward stimulated Brillouin scattering and optomechanical non-reciprocity in standard polarization maintaining fibres. *Light Sci. Appl.* **10**, 119 (2021).

50. Saha, K., et al. Chip-scale broadband optical isolation via Bragg scattering four-wave mixing," CLEO: pp. QF1D–2 San Jose, CA (2013).

51. Hua, S. et al. Demonstration of a chip-based optical isolator with parametric amplification. *Nat. Commun.* **7**, 13657 (2016).

52. Agrawal, G. P. *Nonlinear Fiber Optics* (Academic Press, 2012).

53. Bahabad, A., Murnane, M. M. & Kapteyn, H. C. Quasi-phase-matching of momentum and energy in nonlinear optical processes. *Nat. Photon.* **4**, 570–575 (2010).

54. Supradeepa, V. R. Stimulated Brillouin scattering thresholds in optical fibers for lasers linewidth broadened with noise. *Opt. Express* **21**, 4677–4687 (2013).

55. Huang, B., Wang, J. & Shao, X. Fiber-based techniques to suppress stimulated Brillouin scattering. *Photonics* **10**, 282 (2023).

56. Halder, A., et al. FEM Analysis of a highly birefringent modified slotted core circular PCF for endlessly single mode operation across E to L Telecom Bands. *JEOS:RP*, **20** (2024).

57. Senior, J. M. *Optical Fiber Communications: Principles and Practice* (Prentice-Hall, 2008).

58. Liu, K., et al. Integrated tunable two-point-coupled 10-meter 336 million q coil-resonator for laser stabilization, Frontiers in Optics, pp. FM6D–FM66, (2023).

59. Inoue, K. & Okuno, M. Coherent Anti-Stokes Hyper-Raman Spectroscopy. *Nat. Commun.* **16**, 306 (2025).

60. Ito, F., Fan, X. & Koshikiya, Y. Long-range coherent OFDR with light source phase noise compensation. *J. Light. Technol.* **30**, 1015–1024 (2011).

61. Lu, H.-H., Liscidini, M., Gaeta, A. L., Weiner, A. M. & Lukens, J. M. Frequency-bin photonic quantum information. *Optica* **10**, 1655–1671 (2023).

62. Butcher, J. C. Numerical Methods for Ordinary Differential Equations. 3rd ed., (Wiley, 2016).

Acknowledgements

Author contributions

Conceptualization: G.B., A.A. Experimental: G.B. Analysis: G.B. Discussions and consulting: A.E., M.T. Supervision: A.A. Writing—original draft: G.B. Writing—review & editing: G.B., A.E., M.T., A.A.

Competing interests

The authors declare no competing interests.

Additional information

Supplementary information The online version contains supplementary material available at
https://doi.org/10.1038/s41467-025-62025-0.

Correspondence and requests for materials should be addressed to Ady Arie.

Peer review information *Nature Communications* thanks the anonymous reviewers for their contribution to the peer review of this work. A peer review file is available.

Reprints and permissions information is available at
http://www.nature.com/reprints